ELSEVIER

Ceramics International 27 (2001) 171–177

CERAMICS INTERNATIONAL

Thermal shock strength of Al_2O_3 by laser irradiation method

Shigeru Akiyama [a], Shigeyasu Amada [b,*]

[a] *Ship Research Institute, 6-38-1, Shinkawa, Mitaka, Tokyo 181-0004, Japan*
[b] *Department of Mechanical Engineering, Gunma University, 1-5-1, Tenjin, Kiryu, Gunma 376-8515, Japan*

Received 26 April 2000; received in revised form 9 May 2000; accepted 22 May 2000

Abstract

Various structural ceramics have been developed as heat-resistant materials. It is very important to investigate their thermal shock characteristics. This report presents a newly developed, laser irradiation method to evaluate thermal shock strength and proposes that a critical power density can be a new measure to evaluate heat resistant materials.

The temperature and thermal stress distributions of the cylindrical shaped Al_2O_3 ceramics under irradiation by CO_2 laser beams are analyzed using FEM. The maximum tensile and compressive stresses are obtained with respect to beam diameters for various power densities. These relations lead to critical power densities at which materials are fractured. The relationships between the critical power density and beam diameters derive critical fracture curves which gives the fracture criterion of ceramics. Finally, the irradiation experiments were carried out and their results got a good agreement with the theoretical fracture criterion. It was concluded that the critical fracture curve can be a new measure to evaluate thermal shock resistance of ceramics.

Keywords: C. Thermal shock resistance; D. Al_2O_3; Laser irradiation; Critical fracture curve

1. Introduction

The developments of new functional materials with a high thermal shock resistance have a key technology for space planes, fusion reactor, gas turbines and so on. If these materials, probably structural ceramics, are developed, they will also contribute to other heat engines. In these applications, they will be exposed to very high temperature and high heat-flux environments. So, the thermal shock resistance is critical to select suitable material from the candidate ones. At present a quenching method with the Davidge-and-Tappin-plot [1–3] has been widely and effectively used to evaluate the thermal shock strength of ceramics. The details of this technique have also been discussed in a number of studies [4–6].

Some new evaluation approaches have been proposed, which use a different heating source. Takahashi et al. [7,8], Akiyama and Amada [9] proposed the laser irradiation technique to evaluate the thermal shock resistance of ceramics. They derived the critical power density which corresponds to the critical temperature difference for the quenching method. Recently lasers were applied to the evaluation of the erosion of graphite–carbon fibre composites [10], of the damage of Kelvar 49-epoxy composite[11] and of the fracture of partially stabilized zirconia[12].

This paper presents a laser irradiation method to evaluate of thermal shock strength of Al_2O_3 ceramics and derive a critical fracture curve which defines a fracture criterion for thermal shock. The obtained fracture curves can give a new measure to evaluate thermal shock resistance. Finally, the critical fracture curve derived from the finite element method (FEM) analysis is compared with the laser irradiation experiments.

2. Experimental procedure

The experimental apparatus to evaluate thermal shock resistance is shown in Fig. 1. The system consists of a CO_2 laser, an NC controller which specifies laser power, beam diameter and duration, acoustic emission (AE) sensors and an AE signal counter. The AE sensor can detect a signal when the crack is generated in the specimens. We identify the specimen fracture based on this condition. The shape of the specimen is a cylinder

* Corresponding author. Tel.: +81-0277-30-1549; fax: +81-0277-30-1553.
E-mail address: amada@me.gunma-u-ac.jp (S. Amada).

0272-8842/01/$20.00
PII: S0272-8842(00)00058-4

of 50 mm in diameter and 10 mm in height. A specimen is irradiated by the laser whose power density increases from a lower level until a fracture signal is measured. When the specimen is fractured, we define its power density by the critical one. Beam diameter change from 1 to 60 mm and the beam duration is fixed in 1 s.

3. Analytical model

The cylindrical Al_2O_3 ceramics is irradiated by the laser beam with uniform power density P W/mm^2 and beam diameter D mm, as shown in Fig. 2. The mechanical and physical boundary conditions for the model are given in Fig. 3. The heat transfer coefficients [13] $\alpha_1, \alpha_2, \alpha_3$ for the top, bottom and side surfaces are given in Table 1. The physical and mechanical properties of Al_2O_3 are assumed to be independent of temperature. The initial temperature of the specimen and ambient gas is 20°C. The laser pulse lasts 1 s as shown in Fig. 4. After the laser is cut off, the irradiated surface is cooled down by convection of the ambient gas and by diffusion of heat into the deeper and wider regions of the specimen. The mechanical and physical properties of Al_2O_3 are given in Table 1. The tensile strength σ_t is evaluated from the three-point bending strength σ_b by [14].

$$\frac{\sigma_t}{\sigma_b} = \left[\frac{1}{2(m+1)}\right]^{1/m} \tag{1}$$

where m is the Weibull coefficient and $m = 10$ is used [14] in this calculation. Emissivity for the Al_2O_3 specimens is adopted to be 0.95 [15].

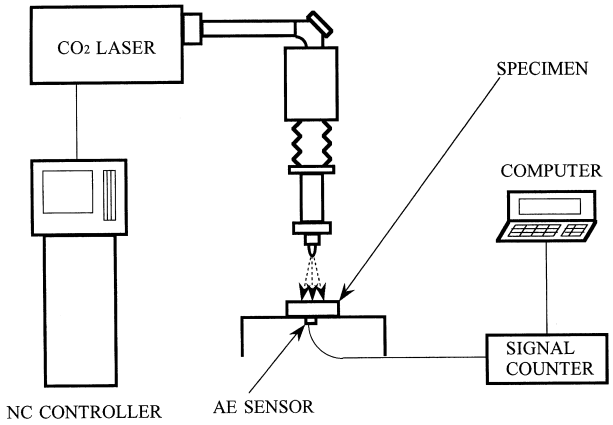

Fig. 1. Experimental apparatus.

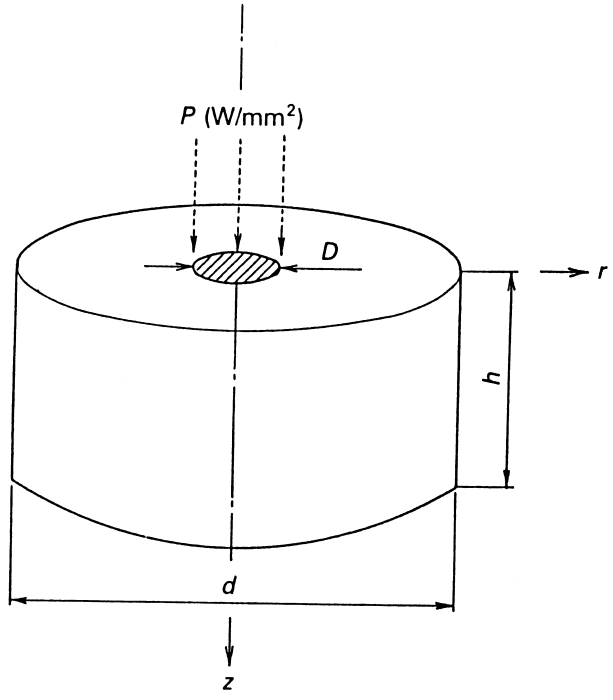

Fig. 2. Analytical model.

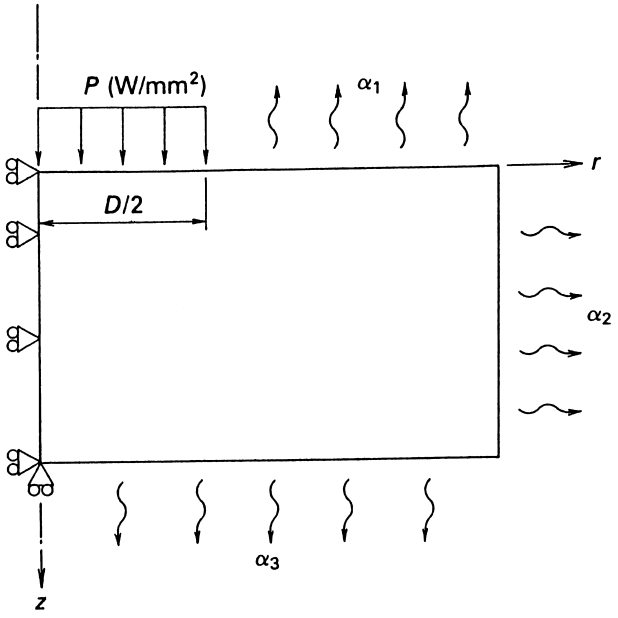

Fig. 3. Boundary conditions for model.

Table 1
Physical properties of Al_2O_3 and heat transfer coefficients[a]

Density	3.9×10^3 kg/m^3
Coefficient of thermal exp.	8.1×10^{-6} /K
Thermal conductivity	8.37 W/(m·K)
Specific heat	0.796×10^3 J(kg·K)
Tensile strength	226 Mpa
Bending strength	392 Mpa
Compressive strength	2550 Mpa
Young's modulus	353 Gpa
Poisson's ratio	0.25
Emissivity (:10.6 μm)	0.95
Heat transfer coefficients (air) W/(m^2·K)	
Top horizontal surface	$\alpha_1 = 1.32\ (\Delta T/L)^{1/4}$
Vertical surface	$\alpha_2 = 1.42\ (\Delta T/L)^{1/4}$
Bottom horizontal surface	$\alpha_3 = 0.61\ (\Delta T/L)^{1/4}$

[a] $\Delta T = (T_w - T_\infty)$ (K); T_w = average wall temperature (K); T_∞ = main stream temperature (K); L = characteristic length (m).

The heat conduction and thermal stress problems are solved by FEM assuming the uncoupled and quasi-static states. Although the beam mode of CO_2 laser is a Gaussian, an uniform distribution is adopted for simplicity of the FEM calculations.

4. Heat conduction analysis

The maximum temperature arises at the beam centre on the irradiated surface. Its time history for a power density 3 W/mm^2 is shown in Fig. 5 with changing the beam diameters. The maximum temperature varies abruptly just after the beginning and cut-off of the laser irradiation. The temperature with time changes almost the same as for any beam diameter above $D=10$ mm during the heating process and above $D=20$ mm during the cooling process.

The temperature distributions with respect to the radius are given in Fig. 6 at 1 s irradiation with $P=3$ W/mm^2. It can be seen that the temperature drops abruptly in the neighbourhood of the beam periphery, and stays flat inside and outside the beam.

Fig. 7 shows the temperature distributions in the depth direction along the centreline of the laser beam for various diameters. The temperature decreases suddenly

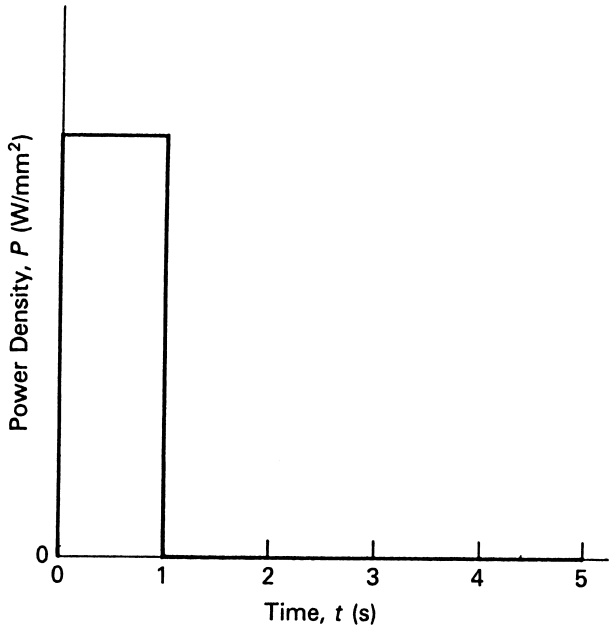

Fig. 4. Duration of laser pulse.

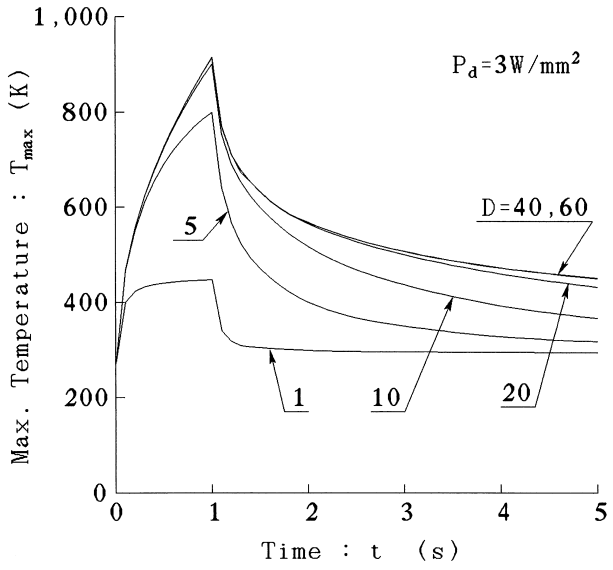

Fig. 5. Time history of maximum temperature.

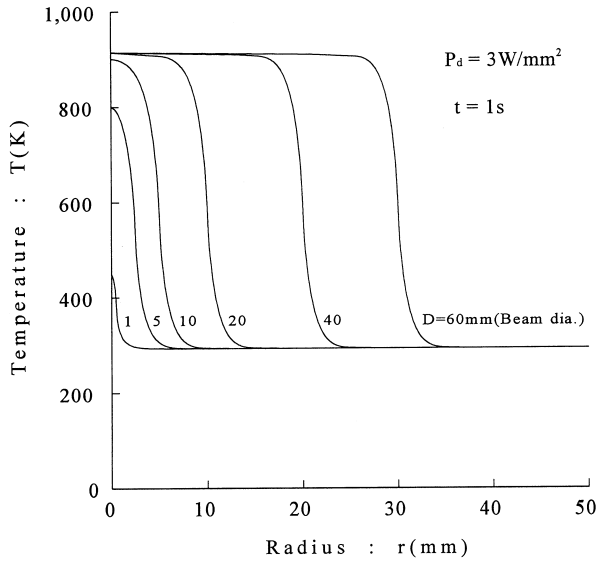

Fig. 6. Temperature distributions in radial direction on irradiated surface for a power density $P_d=3$W/mm^2 as a function of beam diameter at time, $t=1$s.

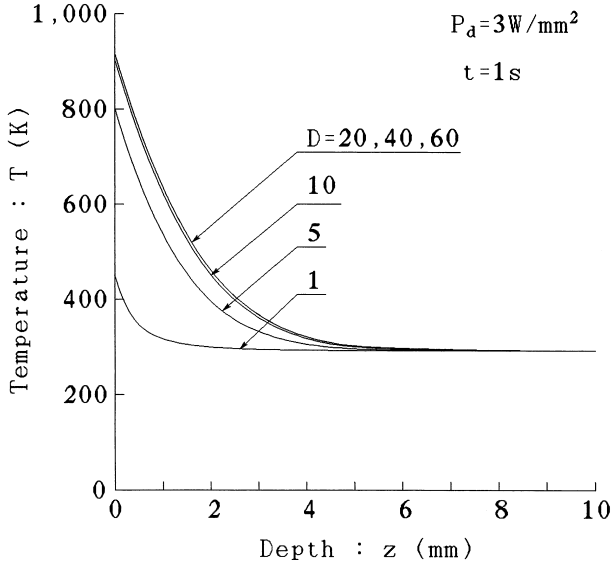

Fig. 7. Temperature distributions in depth direction along centreline.

in the surface layer and does not change so much in the deep region.

5. Thermoelastic stress analysis

The thermoelastic stresses are analysed by FEM using the obtained temperature distributions. The results are shown for the power density $P=3$ W/mm^2 at the moment of 1 s when the maximum tensile stress takes place. Fig. 8 gives the radial stress distributions on the irradiated surface. They are compressive in the entire irradiated surface and their maximum value attains at the beam center.

The hoop stress distributions on the irradiated surfaces are shown in Fig. 9. with respect to radius. They are compressive inside the irradiated circle and change to the tensile stress just outside it. The maximum tensile stress occurs about 6 mm away from the beam periphery and approaches zero with an increase of the radius of the beam on the sample. Under the beam diameter $D=60$ mm, its value becomes 83 MPa. Since ceramics generally fracture due to tensile stress, this fairly large tensile stress may cause thermal stress fracture.

Fig. 10 shows the hoop stress distribution along the depth. They get the maximum compressive value on the irradiated surfaces, and they change to tensile from compressive below 3 mm in depth. The maximum tensile stress takes place in the 3–7 mm depth. For $D=40$ mm, it reaches 165 MPa which becomes much larger than the values occurring on the irradiated surfaces.

Of interest, is where the maximum tensile stress occurs, because it may cause the thermal stress fractures. In the case of $P=3$ W/mm^2, the position of the maximum tensile stress generated in the specimens are marked by a circle in Fig. 11 for various beam diameters. It indicates that the maximum tensile stress occurs on the centreline of the cylindrical specimen in a small beam diameter. On the other hand, it takes place in about 2.8 mm deep for the larger beam diameter than 10 mm. Furthermore, it moves outward with increase of

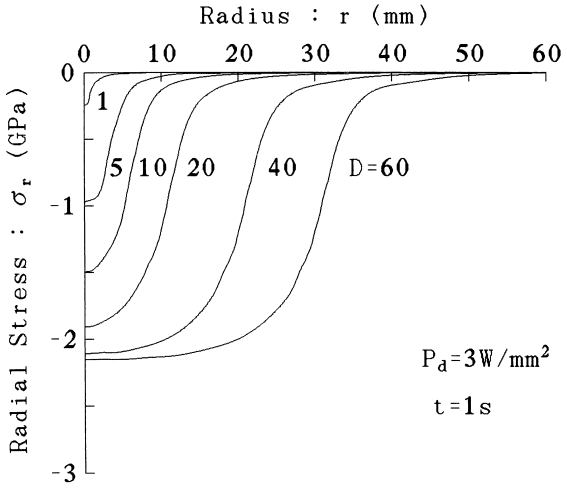

Fig. 8. Radial stress distribution in radial direction on irradiated surface.

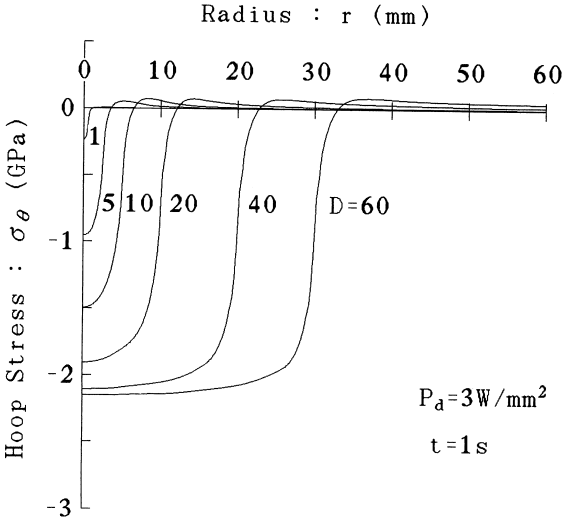

Fig. 9. Hoop stress distribution in radial direction on irradiated surface.

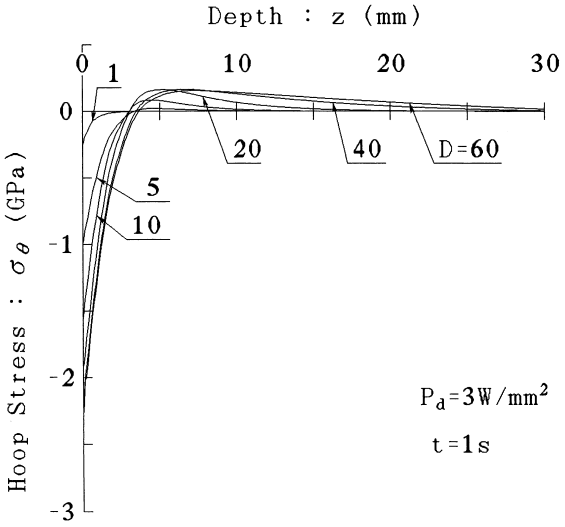

Fig. 10. Hoop stress distribution in depth direction along centreline.

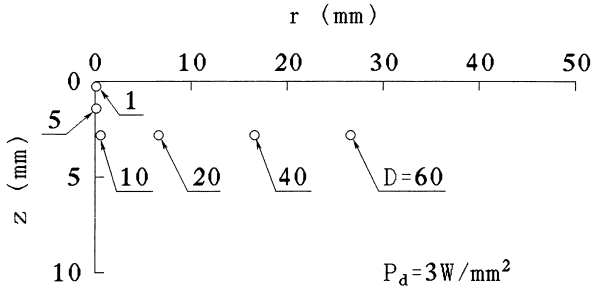

Fig. 11. Position of maximum tensile stress occurred.

beam diameter. If Al_2O_3 is assumed to be fractured due to tensile stress, the specimen subjected to a laser pulse irradiation is initiated to failure at these inside places rather than at the irradiated surfaces.

6. Critical power density

The maximum tensile and compressive stresses are plotted in Figs. 12 and 13, respectively with respect to the beam diameter for various power densities. Adopting $\sigma_t = 226$ MPa for the tensile strength of Al_2O_3, we can draw a horizontal line at $\sigma_{max} = 226$ MPa in Fig. 12. Then each intersection of its line with σ_{max}~D curves gives the critical point at which the alumina specimen is fractured. The power density on the critical points are defined by the critical power density with notation of P_c.

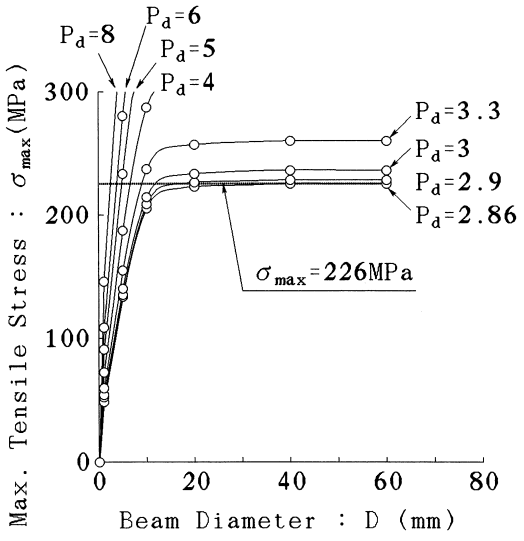

Fig. 12. Relation between maximum tensile stress and beam diameter.

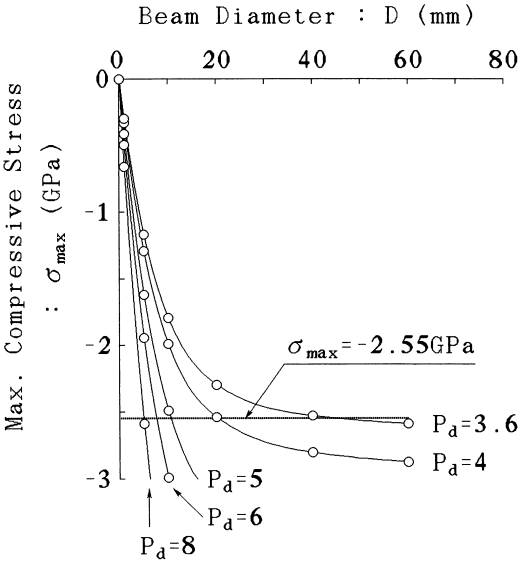

Fig. 13. Relation between maximum compressive stress and beam diameter.

Fig. 13 shows the relation between the maximum compressive stresses and beam diameter for various power densities. If we assume −2500 MPa for the compressive strength of Al_2O_3, we can draw a horizontal line at $\sigma_{max} = -2550$ MPa. Again each intersection of this line with σ_{max}~D curves gives us the critical states at which the alumina specimens are fractured. The obtained P_c from Figs. 12 and 13 is plotted with beam diameter in Fig. 14. These two curves are essentially the fracture criterion for thermal shock strength based on the two different fracture criterions. The region above the critical fracture curve corresponds to the fracture zone. Since the fracture curve for the tensile stress criterion is located under the one on the compressive stress criterion, the tensile stress criterion should be taken into the consideration for a design of alumina components.

The fracture curve given in Fig. 14 decreases considerably in the small beam diameter and approaches asymptotically to a constant value, which is denoted by the asymptotic critical power density P_L. Since P_L is independent of beam diameter, it becomes a measure to evaluate the thermal shock resistance of materials. For Al_2O_3 P_L is about 2.9 W/mm^2 for tensile stress criterion which is higher than $P_L = 0.6$ W/mm^2 for the machinable ceramics MACOR [9].

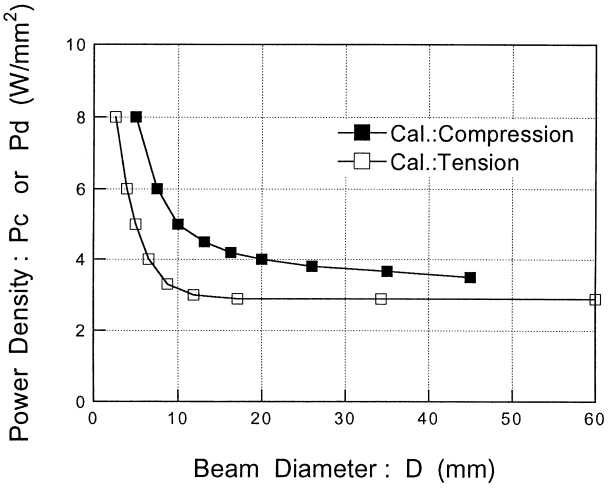

Fig. 14. Critical fracture curve under thermal shock condition.

Table 2
Chemical compositions of Al_2O_3

Chemical compositions (wt.%)					
Al_2O_3	MgO	CaD	SiO_2	Na_2O	Fe_2O_3
99.6	0.15	0.08	0.07	0.05	0.01

7. Thermal shock tests

In accordance with the procedure in Section 2, thermal shock tests were carried out for the Al_2O_3 specimens the chemical compositions of which are given in Table 2. The pulsed and defocused CO_2 laser beams with beam diameter 1–60 mm were irradiated on the specimen surface increasing the laser power from a lower level until the specimen is fractured. The AE sensor was used to detect the crack initiation. The irradiated surfaces were observed with an optical and scanning electron microscope (SEM), simultaneously for the confirmation of the AE detection.

The SEM photographs of the irradiated surfaces are shown in Fig. 15 for the critical power density $P=3.5$ W/mm^2, Fig. 16 for $P=3.0$ W/mm^2 and Fig. 17 for $P=2.8$ W/mm^2, with a fixed beam diameter $D=10$ mm. It was observed in these figures that the higher critical power density leads to the larger crack size in the specimens.

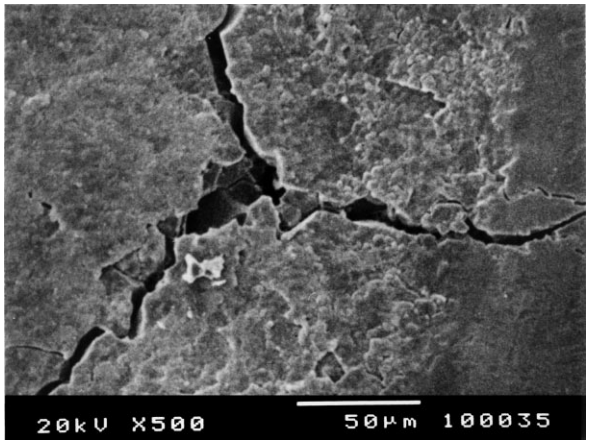

Fig. 15. SEM photograph of irradiated surface near the beam periphery with $P=3.5$ W/mm^2.

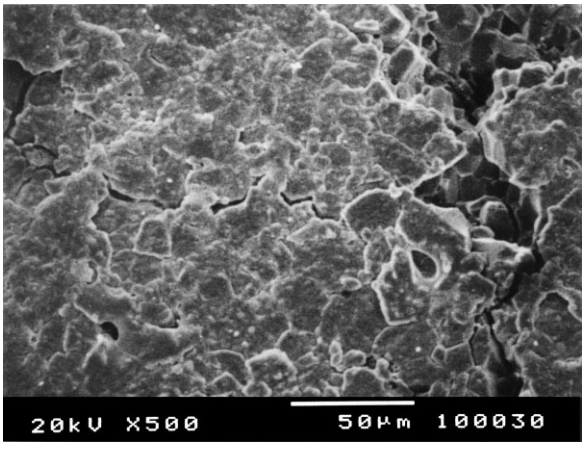

Fig. 16. SEM photograph of irradiated surface near the beam periphery with $P=3.0$ W/mm^2.

The critical power density P_c at which the cracks were initiated was obtained and plotted in Fig. 18. White circles indicate P_c without cracks and solid circles P_c with cracks. These results showed that the critical power density curves derived from both the tensile stress criterion of FEM analysis and the experiments are in good agreement.

It was concluded that the critical power density P_c which can cause the specimen fractures can be a measure of thermal shock resistance of materials. Since P_c depends on beam diameters, P_L corresponding to a constant P_c with respect to beam diameters is recommended to be used for the evaluation of thermal shock resistance.

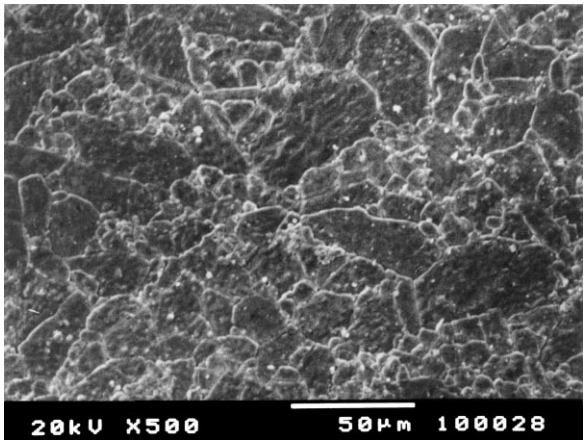

Fig. 17. SEM photograph of irradiated surface near the beam periphery with $P=2.8$ W/mm^2.

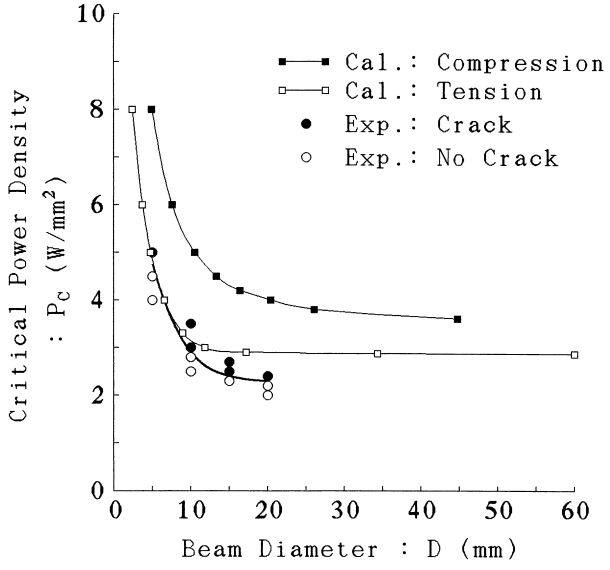

Fig. 18. Comparison of critical fracture curve based on theory with experiments.

8. Conclusions

Comparing with the traditional quenching method to evaluate thermal shock resistance of structural ceramics, a new, simple highly accurate approach was developed based on laser irradiation. For the Al_2O_3 ceramics heated by CO_2 laser beam, the quasi-stationary thermoelastic stresses were analysed by FEM based on the uncoupled assumption, and the thermal shock experiments were performed with a CO_2 laser. The following conclusions were obtained.

1. The maximum tensile stress is generated in the place just outside the beam periphery on the irradiated surface.
2. Using a fracture criterion the critical fracture curve was obtained theoretically, which specifies the critical power density-beam diameter relation.
3. The theoretical critical fracture curve agreed well with the one obtained from the experiments.
4. An asymptotic critical power density P_L can be used to evaluate thermal shock resistance of ceramics. P_L of Al_2O_3 is about 2.9 W/mm^2 for tensile and 3.6 W/mm^2 for compressive failure for the geometry and test condition of this study.
5. P_L can be a measure of thermal shock resistance.

References

[1] J.P. Singh, J.R. Thomas, D.P.H. Hasselman, Analysis of effect of heat-transfer variables on thermal stress resistance of brittle ceramics measured by quenching experiments, J. Am. Ceram. Soc. 63 (1980) 140–144.

[2] D.P.H. Hasselman, Unified theory of thermal shock fracture initiation and crack propagation in brittle ceramics, J. Am. Ceram. Soc. 52 (1969) 600–604.

[3] D.P.H. Hasselman, Strength behavior of polycrystalline alumina subjected to thermal shock, J. Am. Ceram. Soc. 53 (1970) 490–495.

[4] P.F. Becher, D. Lewis, K.R. Carman, A.C. Gonzalez, Thermal shock resistance of ceramics: size and geometry effects in quench tests, Ceram. Bull. 59 (1980) 542–545.

[5] T. Gao, N. Nishikawa, M. Hibino, M. Takatsu, Temperature dependence of so-called heat transfer coefficient under thermal shock test, J. Ceram. Soc., Japan 101 (1993) 788–792.

[6] T. Sakuma, U. Iwata, H. Takaku, Evaluation of thermal shock resistance of ceramics, Trans. Japan Soc. Mech. Eng., Ser. A 57 (1991) 2741–2746.

[7] S. Takahashi, Fracture evaluation of functionally graded materials, Powder and Powder Metall. 37 (1990) 913–917 (in Japanese).

[8] T. Hashida, T. Ishikawa, T. Tobe, S. Takahashi, Development of a laser heating method for evaluating thermal shock/fatigue resistance of ceramic thermal barrier coating for gas turbine blade, Trans. JSME, Ser. A 58 (1992) 15–19.

[9] S. Akiyama, S. Amada, A new method to evaluate the thermal shock resistance of ceramics by laser pulse irradiation, Fusion Technol. 23 (1993) 426–434.

[10] H. Brinskschulte, E. Desksnis, Heat shock resistance of graphite determined with a CO_2 laser, J. Nucl. Mater. 155–157 (1988) 261–266.

[11] R.J. Morgan, F.-M. Kong, J.K. Lepper, J. Compos. Mater. 22 (1988) 1026–1044.

[12] M. Itou, K. Ueda, T. Sugita, Fracture mechanics analysis of thermal shock cracking of ceramics in laser heating, J. Soc. Prec. Eng. 58 (1990) 1487–1492.

[13] I. Tanishita, Heat Transfer, Shoukabo Press, Japan, 1988, pp. 155–156.

[14] Ceram. Soc. Japan, Mechanical Properties of Ceramics, Japan Ceram. Soc., 1988, pp. 23–25.

[15] Y.S.Touloukian, D.P. Dewitt, Thermo-Physical Properties of Materials, Vol. 8, IFI/Plenum, 1972, p. 149.